ISSN: 2639-0108

Research Article

Advances in Theoretical & Computational Physics

Designing TiC@GNPs reinforced pure Ti matrix composites by mechanochemical ball milling and semi-solid sintering

Zai-Yu Zhang[1],[2]*, Jian-jun Yang[3], Yuan Yang[1] , Liang Cao[1], Zai-Qi Zhang[1]*

[1]Hunan Provincial Key Laboratory of Dong Medicine, Hunan University of Medicine, Huaihua 418000, China

[2]School of electronic and information engineering, Anshun University, Guizhou, Anshun 561000, of China

[3]College of Materials and Advanced Manufacturing, Hunan University of Technology, Zhuzhou 412007, China

***Corresponding author:**
Zai-Yu Zhang, Hunan Provincial Key Laboratory of Dong Medicine, Hunan University of Medicine, Huaihua 418000, China.

Submitted: 10 Jan 2023; **Accepted:** 23 Jan 2023; **Published:** 10 Feb 2023

Citation: Zhang, Z. Y., Yang, J. J., Yang, Y., Cao, L., Zai-Qi Zhang, Z. Q. (2023). Designing TiC@GNPs reinforced pure Ti matrix composites by mechanochemical ball milling and semi-solid sintering. *Adv Theo Comp Phy,* 6(1), 42-52.

Abstract

In this work, we report on a novel in-situ TiC nanoparticles sticking to graphene nanoplatelets (TiC@GNPs) reinforced titanium matrix composites. In-situ TiC nanoparticles are produced in both mechanical ball milling and sintering processes. Ultrafine composite powder is obtained by mechanochemical ball milling from refined pure titanium powder and graphene nanoplatelets (GNPs) .A new type of TiC@GNPs/Ti composite materials with high strength and toughness and three-dimensional network distribution are made of ultrafine composite powder by various curing methods. The effects of different hot pressing parameters and reinforcing phase content on the microstructure and mechanical properties of the composites were studied. The results shown that the strength and plasticity of the ultrafine TiC@GNPs/Ti composites prepared by hot pressing sintering are obviously improved compared with the matrix. The strengthening mechanism of composites is mainly the synergistic effect of fine grain strengthening and dislocation strengthening. The ductility is due to grain refinement and in situ layered structure of TiC@GNPs particles. This layered structure is a double-scale microstructure, which is characterized by the lamellar composed of ultrafine bcc-Ti and ultrafine GNPs surrounding the fine crystal equiaxed fcc second phase TiC. The in-situ synthesis of nano-tic and nano-GNPs synergistic growth shows a criss-cross in the microstructure. The three-dimensional network distribution of GNP in titanium matrix can regulate the contradiction between strength and plasticity of titanium matrix composites.

1. Introduction

Discontinuous reinforced titanium matrix composites (DRTMCs), featuring higher service temperature and better plasticity and processability than traditional titanium alloys, have attracted extensive attention in the past decades [1-6]. Many researchers have prepared systems of DRTMCs with different enhancement phases and methods, but most of the enhancement phases in DRTMCs are uniformly distributed [7-11]. However, uniform distribution of reinforcing phases can only achieve a limited reinforcement effect and lead to a significant reduction in the plasticity of the composites, especially for powder metallurgy materials, which exhibit a high room temperature brittleness [10]. It has been shown that the network-like non-uniform distribution of the reinforcement phase can effectively solve the problem of high powder metallurgy brittleness at room temperature, which can improve the hardness and strength, but reduce the plasticity slightly [12-15].

The three-dimensional Mesh structure conforms to the hard phase surrounded soft phase structure corresponding to the performance upper limit in Hashin-Shtrikman (H-S) theory, and has a good prospect in the field of metal matrix composite [16-17]. In this paper, we designed TiC@GNPs reinforced titanium matrix composites (TiC@)GNPsTMCs) with a non-uniform three-dimensional Mesh distribution. Specific design ideas are as follows：Firstly，the composite powder was prepared by mechanical chemical ball milling process from high purity flake graphite and pure titanium powder. Secondly, the new TiC@GNPsTMCs were prepared by vacuum warm pressing forming, vacuum hot pressing sintering and atmospheric hot rolling. During the whole preparation process, mixed sintering of powders with different grain sizes, semi-solid sintering and recrystallization induced by plastic deformation and low temperature heat treatment were realized, which made the nano-TiC and GNPs grow in the titanium matrix in a coordinated way. Finally, the two nano-particles form a three-dimensional network with alternative hardness, which makes the new composite have good mechanical properties. It provides a new idea to solve the problem of high strength and low plasticity of metal composite materials.

2. Experimental Process

The whole material preparation process in this work is shown

in Figure 1, which is mainly composed of mechanical chemical ball milling process, semi-solid sintering process and hot rolling process. The specific experiment details are as follows:

2.1. Mechanical and chemical ball milling

Mechanical ball milling is an effective method of dispersing and mechanical alloying in a relatively closed space. It can effectively prepare various metal - based amorphous nano - composite powders. Unless high-energy ball milling can destroy graphene's two-dimensional structure and produce defects, it can even convert graphene into amorphous carbon over a long period of time. Unlike high-energy ball mills, low-energy ball mills can effectively mix graphene evenly with the metal matrix without causing significant damage to the graphene. At the same time, low energy ball milling can also solve the agglomeration problem that often occurs in the preparation of metal matrix composites with graphene and other nano-particle reinforcers, and realize the process of atomic diffusion, solid state reaction or phase transformation, etc., which is a material preparation method for preparing nano-powders, alloys or compounds [19]. In this paper, three ball milling processes including short time high energy ball milling, long time low energy ball milling and chemical solution ball milling are used to prepare composite powder materials.

2.1.1. Refinement of titanium powder

Titanium powder with particle size of 30 μm and 10g of 100 μm (10 g for each of them) were used as the raw material. They were put into a 300 ml stainless steel ball mill tank along with 200 g balls and added with 100 ml ethanol. Pure titanium powder was obtained by the mixing two particle sizes of pure titanium powder with equal mass using QM-QX planet ball mill produced by Nanjing Nanda Instrument Factory. In this process, sodium stearate was used as the process control agent to promote the fracturing of Ti particles in the process of cold welding. The ball milling process was protected by argon gas, and the powder was kept from overheating by alternately milling for 30min and stopping for 10 min. Secondly, on the basis of refining pure titanium powder by dry milling, anhydrous alcohol was added into the spherical tank for wet ball milling, and steel ball milling medium with corresponding radius was used at the same time. Finally, pure titanium mixed mud was formed after corresponding high-energy ball milling and low-energy ball milling for 2 hours each. The titanium slurry was dried at 100℃ for 24h in a vacuum drying oven to get pure titanium powder for later use.

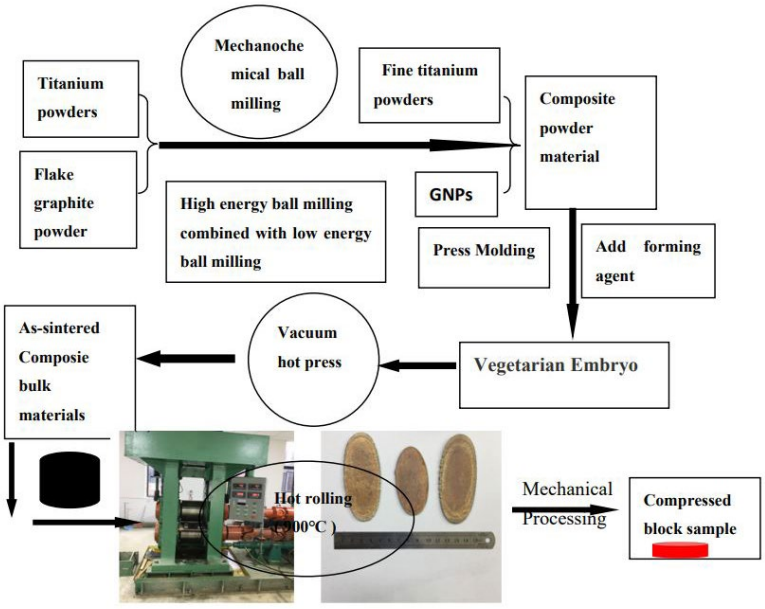

Figure 1: Experimental technology roadmap in this work

2.1.2. GNPs preparation

A mixture of 0.5 g flake graphite, 2g ammonium chloride and different volumes of glacial acetic acid was added to a steel ball mill tank containing 10 steel balls (weight 5 g, diameter 10 mm). High speed ball grinding (400 rpm) for 10 hours. The sample was then taken out and ground for 20min, and placed in the air for 48 hours to volatilize glacial acetic acid. Then remove 2 g of the above powder subject to mill the ball at a low speed (150 rpm) for 24 hours. The powder was treated by ultrasonic for 2 hours in deionized water/anhydrous ethanol (volume ratio 1:3) (1000 ml) at room temperature, then centrifuged at a speed of 3000 RPM for 10 minutes, and the supernatant was removed. The supernatant was subjected to centrifuge again at 8000 RPM for 5 min. The precipitation products were retained and placed in a vacuum dryer (vacuum degree 0.5mpa) at room temperature, and finally the GNPs samples needed were obtained.

2.1.3. Preparation of composite powder

The refined pure titanium powder and GNPs prepared were placed in anhydrous alcohol for ultrasonic dispersion for 30 min to obtain GNPs/Ti composite mud. Then wet ball milling was used, and the ball milling process was combined with high and low energy ball milling. In order to prevent air pollution, the whole mixing and filling process is carried out in a glove box filled with argon gas, using a steel ball mill tank with a volume of 500 ml and an inner diameter of 100 mm. The whole high speed ball mill adopts steel ball as grinding medium, and the ball powder ratio is 10:1. The ball milling process is protected

by vacuum, and the powder is ground for 30min and stopped for 10min alternately to avoid overheating. 400 RP high energy ball milling for 1h and 150RP low energy ball milling for 2h. The composite mud was placed in a vacuum drying oven and dried at 100℃ for 24h. All the above powder and mud transfer is done in an argon glove box to prevent any atmospheric contamination. Suitable zinc stearate was added into the composite powder slurry as a subsequent forming control agent. According to the design of this work, two kinds of powder for semi-solid sintering was used, namely pure titanium powder and composite powder containing GNPS 0.5%. The ball milling parameters of mechanical alloying processes used in the above three processes are shown in Table 1.

Table 1: Ball-milling conditions used for mechanical alloying

Ball milling project	Condition
Ball mill tank	stainless steel
Grinding ball	stainless steel
Initial powder	Ti powder (99.5%pure, 30-100 μm) Flake graphite powder (99.9%pure, 10 μm Below)
Speed	speed High speed 400rpm; Low speed 150rpm
Ball material ratio	10:1
Ball milling time	10-60h
Process control agent	Stearic acid (1wt%)
Ball milling environment	High purity argon (99.999%)

2.2. Preparation of composite materials

The composite powder prepared in 2.13 is used as raw material. After adding a certain forming agent, the semi-solid sintered original blank samples are pressed mechanically at a pressure of 500MPa. Vacuum hot pressing sintering system is adopted for raw raw material samples, protected by high purity Ar gas. The whole sintering process is completed by solid sintering and semi-solid sintering. (1) Solid sintering: A 10 g raw blank sample was wrapped with Ta paper about 28 mm thick and placed in a graphite mold with an inner diameter of 15 mm. It was premolded at 20 MPa and then placed in the furnace chamber under pressure to 30 MPa. The temperature was heated to 1050 ℃ at a rate of 100 K/min (50 ℃ lower than the preferred eutectic transition temperature of a certain two phases in the complex phase system). (2) Semi-solid sintering: In order to prevent extrusion liquid phase, the sintering pressure was reduced from 30 MPa to 20 MPa, and to prevent temperature overshooting, the sintering temperature was raised to semi-solid sintering temperature (1100 ℃) at 50 ℃/min, and then the sintering temperature was kept for 60 min. Then, the power supply was cut off at 20 MPa and the temperature was cooled to 600 ℃. Finally, the sintering pressure was cooled to room temperature without pressure. The sintering process was controlled by thermocouple and the sintering and densification curves were recorded in real time. The same amount of amorphous powder was sintered in solid state at 900 ℃, and also held for 5 min and cooled. The size of the obtained block alloy is 15 mm in diameter and 10 mm in length. For the block composites prepared by the three processes, samples of different sizes were cut by wire, mechanically ground to 2000# and metallographically polished. Kroll corrosion solution was used for metallographic etching. The phase composition of the alloy was determined by D/MAX-2500/PC XRD, and the microstructure and microcomposition of the alloy were observed by XL-30 FEG scanning electron microscopy (SEM) and Tecnai G2 F30 TEM. The microcomputer-controlled electronic experimental machine (CMT5105, MTS) was used for compression experiment. The sample diameter was 3 mm, length was 6 mm, and strain rate was 5×10-4 s-1. Strain was measured with an extensometer and the average of 3 test results was taken for each test result. In this paper, the semi-solid sintered samples are distinguished by numerical combination, such as 0.25-1100-50-60, where 0.25 is the mass content of the enhanced phase TiC@GNPs is 0.25% of the whole mass, 1100 is the sintering temperature of 1100℃, 50 heating rate of 50℃/min, and 60 holding time of 60min. The meanings of other numbers are extrapolated

3. Results

3.1. Amorphous composite powder

In this work, the composite powder containing part of amorphous is obtained, and its specific characteristics are shown in Figure 2. Fig.2 (a) is a scanning electron microscope image of the composite powder, which shows the initial binding state of the original GNP and Ti matrix. It can be seen that the original GNP is disk-shaped, while the GNP in the Ti matrix is folded, indicating that the compatibility between GNPs and titanium matrix is poor. Among them, GNPs is obviously embedded in the titanium matrix. Fig.2 (b) is its transmission image. GNPs and Ti particles are coated with GNPs, which helps prevent Ti agglomeration and can be well dispersed on GNPs. The image shows that GNP is half wrapped around Ti particles and connected to each other to form a network structure. Fig.2 (c) shows HRTEM images and Fourier transform (FFT) spectra of titanium-based amorphous composite powder, from which GNPs and β-Ti can be seen. The black area is pure Ti powder particles. The diffraction ring is calibrated by electron diffraction transform (FFT). The corresponding plane spacing of each diffraction ring is 0.274 nm, 0.241 nm, 0.215 nm, respectively, and the corresponding crystal planes are α -ti :(100), (002), (101). The white snowflake region is cluttered with an amorphous substrate.Fig.2 (d) shows another HRTEM image and Fourier transform (FFT) spectrum of the titanium-based amorphous composite powder, from which it can be seen that the alloy powder contains a large number of amorphous phases and a small amount of nano B-Ti and GNPs. Using amorphous alloy powder as raw material to prepare bulk alloy has the following advantages :(1) amorphous powder has viscous rheological behavior in its crystallization process [18-

20], which is conducive to accelerating densification at low temperature, thus achieving near-total densification; (2) At the same sintering temperature, amorphous powders have shorter grain growth time than crystalline alloy powders of the same composition, which is conducive to fine crystallization [21-23]. (3) Due to the homogeneity of thermodynamic and kinetic conditions, amorphous grains tend to form high-angle grain boundaries and achieve equiaxed crystallization [21-23]. (4) Based on the theory of amorphous crystallization, it is beneficial to realize fine crystallization and structural composite by regulating the nucleation and growth mode of grains in the crystallization process [24-27]. (5) The uniform distribution of fine grains after amorphous crystallization is conducive to the homogenization of a two-phase preferred eutectic transition, and thus to the homogenization of liquid phase caused by eutectic transition.

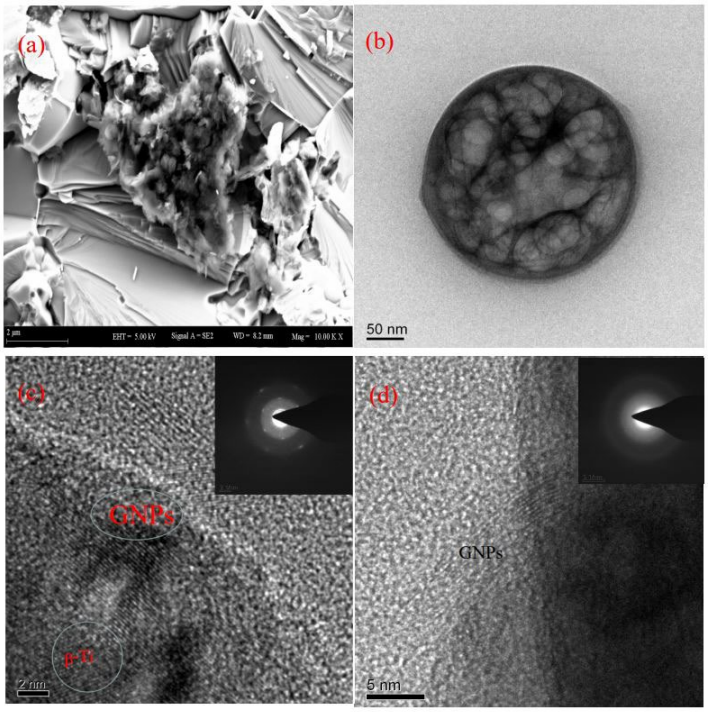

Figure 2: Microstructure characteristics of TiC@GNPs reinforced titanium matrix composite powder materials ((a) is the scanning morphology, (b) is the transmission global image; (c) and (d) are HRTEM images and their Fourier transform (FFT) spectra

3.2. Raman and XRD analysis of sintered samples

Raman spectroscopy can distinguish the structure of ordered and disordered carbon materials, and can also detect and characterize nanoscale GNPs nondestructively and efficiently. Figure 3 shows the Raman spectra of the original composite powder and 0.5wt%TiC@GNPs/Ti composite powder under different sintering conditions. There is no characteristic peak in the Raman spectrum of the original composite powder, indicating that the original powder is amorphous. The three characteristic peaks of GNPs of the composite after vacuum hot pressing and sintering are obvious, among which the G peak is strong and sharp, appearing at 1574.4cm-1, which is a single Lorentz peak, and the defect is not obvious, indicating that the graphite crystallite is high. With the increase of sintering temperature, the peak D of graphite after oxidation significantly increased, indicating that the addition of oxidizer introduced a large number of oxygen-containing functional groups into the graphite sheet originally arranged regularly, resulting in defects and the hybrid transformation from SP2 to SP3. After reduction, there are oxygen-containing functional groups on GNPs.

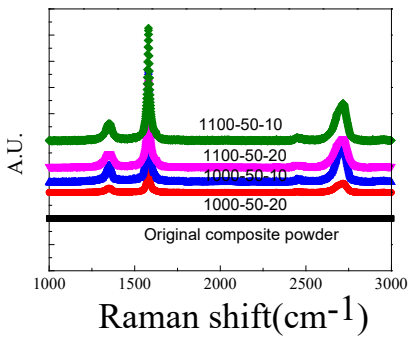

Figure 3: Raman spectra of Fig.3TiC@GNPs/Ti composites under different sintering conditions

In order to analyze the phase composition of semi-solid sintered materials, in situ XRD analysis was performed on the composite materials and pure titanium sintered at 1100°C. In Figure 4, (a) is pure titanium, and (b) is TiC@GNPs/Ti composite. Its phase was calibrated according to PDF#8-004 and PDF#89-3828. On the whole, there are two phases of the composites: TiC and C. Pure titanium is all α-Ti. It indicates that GNPs reacts with titanium in the sintering process to produce TiC and graphene structure. XRD analysis also revealed that titanium in pure titanium samples are hexagonal structure, while TiC and GNPs in composites are cubic structure. The three diffraction peaks of pure titanium samples at 38.5°, 55.7° and 70.4° all come from pure titanium (PDF No. 851326). In addition to the above three characteristic peaks of pure titanium, the graphite diffraction peak at 26.5°, the graphene peak at 11.6° and the TiC peak also appear in the composite powder. This phenomenon indicates the mechanical alloying of graphite and titanium during ball milling. The peak (002) of pure titanium is 38.5°, while that of graphene/titanium is 38.2°. The peak (002) of the composite material is slightly offset, which is due to the solid solution of carbon atoms in graphene into titanium matrix, which mainly causes the expansion of C-axis [24], resulting in lattice distortion, and thus the peak is offset.

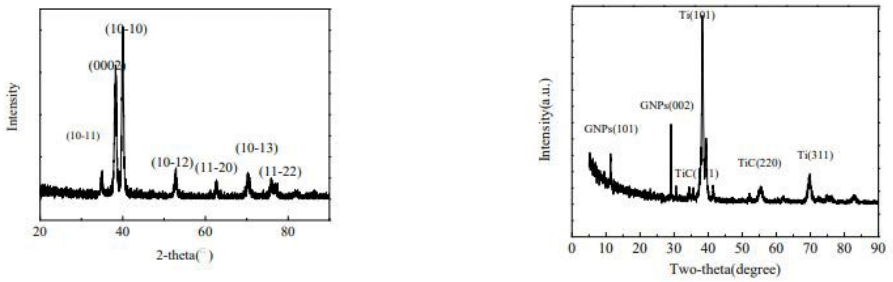

Figure 4: XRD analysis of pure titanium and TiC@GNPs/Ti composites after semi-solid sintering ((a) pure titanium; (b) (TiC@GNPs/Ti composites)

3.3. Compression Performance

In this paper, a microcomputer controlled electronic experimental machine (CMT5105,MTS) is used for compression experiment. The experimental rate is 0.5mm/min. The size of compressed sample is ϕ 4mm*6mm. Three groups of the same sintered samples were prepared for each compression test to ensure the reliability of the data. The compressed samples were obtained by 1100℃ vacuum hot pressing and sintering and then 900℃ hot extrusion.

Figure 5 shows the compressive stress-strain curves of pure titanium samples under different preparation conditions. The compression performance of various samples is summarized in Table 2. Figure 5 shows pure titanium at 900~1100℃, 50℃/min and 60 min. As can be seen from Figure 5, the yield strength, compressive strength and fracture strain of pure titanium materials all show an upward trend with the increase of temperature from 900℃ to 1100℃. Table 2 shows the compressive properties of the composites containing Ti and two reinforcing phases at different holding times of 1000℃ and 1100℃. It can be concluded that for pure titanium, under the condition of constant temperature and heating rate, the longer the holding time, the more strength and plasticity decline. Under the conditions of 1 000℃, 100℃/min and 90min, the compressive strength and fracture strain of Ti samples decreased by nearly 100 MPa and 4% compared with the samples held for 60 min under the same conditions. The compressive strength and ductility of Ti at 1 100℃, 100℃/min and held for 90 min were lower than those at 1 000℃, 100℃/min and held for 60 min. The decrease of compression performance of Ti with increasing temperature and decreasing heating rate may be related to grain coarsening. For the 0.25wt%TiC@GNPs composite, the longer the holding time is at 1 000℃ and 100℃/min, the better the compressive properties of the composite, and the yield strength, compressive strength and fracture strain show an increasing trend. At constant temperature and heating rate, the reaction degree of GNPs and Ti increases gradually with the extension of holding time and the further diffusion of atoms. In this study, the reaction degree of GNPs and Ti increased gradually with the extension of holding time from 60 min to 90 min for samples at 1 000℃ and 100℃/min. The experimental results show that with the increase of the reaction degree of GNPs and Ti, the compression performance first increases and then decreases. It can be inferred that there is an optimal proportion of the reaction degree of GNPs and Ti to obtain the best mechanical properties. For 0.25wt% TiC@GNPs composites, the best compressive properties, yield strength of 1 086 MPa, compressive strength of 1 924 MPa and fracture strain of 41 were found in the sintering conditions of 1 000℃, 100℃/min and 120 min.

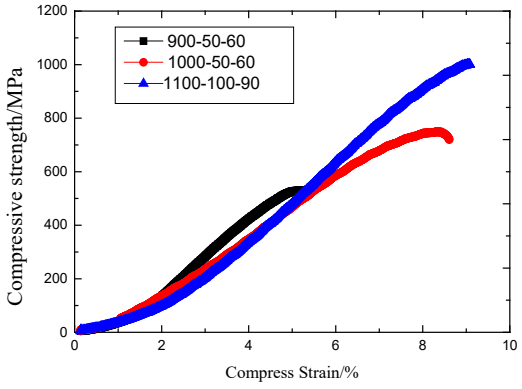

Figure 5: Compressive stress-strain curves of pure titanium samples under different preparation conditions

Table 2: Compressive properties of the TiC@GNPs/Ti and Ti network structure composites under different sintering conditions

Sample	Yield strengthσ0.2 /MPa	Compressive strength σb /MPa	Fracture strainε/%
0.5-900-50-60	1039±5	1509±6	32.8±0.3
0.5-1000-50-60	1091±1	1602±5	35.9±0.4
0.5-1100-50-60	1148±6	1669±5	35.8±0.3
0.25-1100-100-60	1140±4	1742±5	38.9±0.2
0.25-1000-100-90	1056±5	1751±5	39.2±0.5
0.25-1000-100-120	1148±3	1824±5	41.3±0.3
Ti-1000-50-60	987±5	1231±5	9.6±0.4
Ti-1100-100-90	569±5	896±5	5.6±0.2

4. Discussion

The reasons for the increase of strong plasticity of composite materials are analyzed in the following two aspects. One is the compression of microscopic fracture aspect, the other is the coordinated growth of two kinds of microscopic particles TiC @ GNPs.

4.1. Microstructure

Figure 6 shows the compression fracture morphology of 0.25wt% GNPs/Ti under different sintering conditions. Figure 6(a) shows the compression fracture of the sample under 1000°C, 50°C/min and 60 min of insulation. Figure 6(b) shows the compression fracture of the sample under 1000°C, 100°C/min and 90 min of insulation. By comparison, it can be seen that the cross-section of the sample at 100°C/min is smoother, and more dimples and residual GR micro-aggregates can be observed on the surface. However, the fracture surface of the sample at 50°C/min was rough, and the deformed matrix particles could be clearly seen in the section. The fracture extended along the mesh interface, which was similar to "intergranular fracture". The large size matrix particles of 10~20 are not easy to densify in sintering, especially when the sintering temperature is relatively low, reducing the heating rate is equivalent to extending the holding time, which is conducive to atomic diffusion and forming a more solid interface. Fracture surface morphology of samples held at 1 100°C, 50°C/min and 60min as-showed in Figure 6(c) and Figure 6(d). The surface of quasi-dissociation fracture is similar to that of the sample at 1 000°C, and elongated dimples and cleavage steps can be observed. However, a macroscopic crack was observed on the surface of the sample at 1100°C. Within the crack, the fracture surface could be clearly seen along the interface of the network structure, and the network structure as a unit was squeezed to form a very rough fracture surface. Compared with the sample at 1 000°C, the fracture surface showed slightly weaker strength and plasticity. Perhaps due to the further increase of GNP and Ti reaction, GNP residual amount is very small, which limits its excellent carrying capacity.

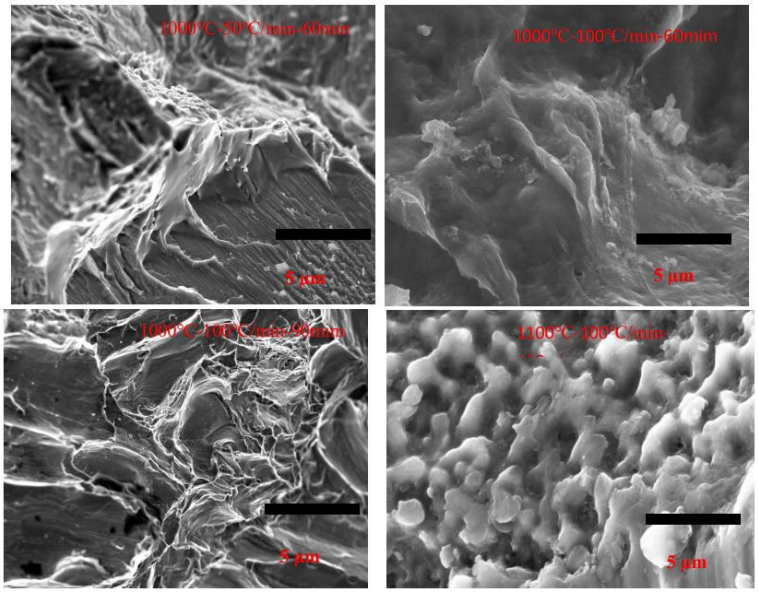

Figure 6: SEM images of the compressive fracture surfaces of 0.25WT% TiC@GNPs/Ti composites under different sintering conditions

4.2. GNPs @ TiC

4.2.1. TiC

As shown in figure 7, the driving force in the phase transformation process comes from the free energy difference (volumetric free energy difference or chemical free energy difference) between the two phases. It is represented by ΔGV. The phase transition resistance is the interface energy generated by the emergence of the new phase embryo. It is represented by γS. Ingeneral, at a certain temperature, ΔGV and γS are a constant, ΔGV is a function of the nucleus radius. There is a critical value in the radius of crystal nucleus: when the radius of crystal nucleus grows up, the free energy of the system will increase, so the crystal embryo at this scale is very unstable, difficult to grow up, and eventually dissolve and disappear. However, as the system increases, the free energy of the system decreases, and the crystal nuclei grow steadily. Therefore, not all crystal nuclei can form stable crystal nuclei, and only those which reach the critical nucleus radius can grow spontaneously, which requires overcoming the critical nucleation work or nucleation barrier. The critical nucleus radius and critical nucleation work can be calculated by formulas $\frac{d\Delta G}{dr}=0$.

$$\Delta G=-\frac{4}{3}\pi r^{3}\Delta G_{V}+4\pi r^{2}\gamma_{S} \quad (1)$$

$$r^{*}=-\frac{2\gamma_{S}}{\Delta G_{V}} \quad (2)$$

$$\Delta G^{*}=\frac{16\gamma_{s}^{3}}{3(\Delta G_{V})^{2}} \quad (3)$$

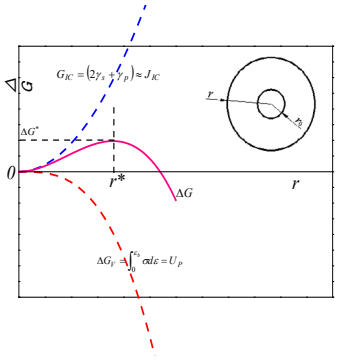

Figure 7: Relationship between free energy of spherical void and its radius

4.2.2. GNPs

It is possible for C to form A GNPs sheet and grow perpendicular to the grain boundary at the α/β interface during the discontinuous desaturation of supersaturated α solid solution. The growth of the new GNPs end towards the parent phase is different from that of the spherical second phase. Now the discussion is as follows:

As shown in Figure 8, the thickness of GNPs sheet is 2r, the end face is circular arc, and the radius is r. The original carbon concentration of α solid solution is C_0, the concentration of new phase β is C_β, and the concentration of α phase at the interface of α/β is ,C_α so the solute atomic carbon will diffuse to the interface, resulting in the GNPs sheet length being larger. Different from the side, the diffusion of solute atoms in the alpha solid solution is not one-way, but the radial. After the end face of GNPs slices extends forward, the carbon concentration of the parent phase on both sides has decreased to C_0 . Therefore, GNPs slices cannot grow laterally and their thickness will not increase. Zener [28] argues that formula (4) is applicable to GNPs growth as long as it is modified. This correction is to make $L=C_{(r)}$, $C_\alpha=C_\alpha(r)$, so the formula (4) can be converted into (5):

$$v=\frac{D(C_0-C_\alpha)}{L(C_\beta-C_\alpha)} \quad (4)$$

$$v=\frac{D(C_0-C_\alpha(r))}{Cr(C_\beta-C_\alpha(r))} \quad (5)$$

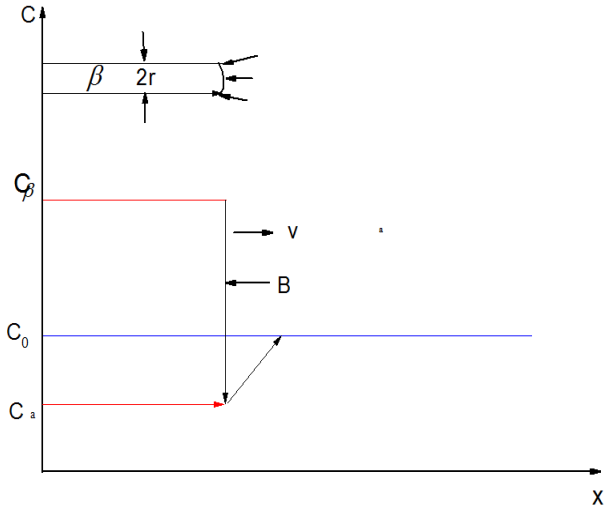

Figure 8: Schematic diagram of the new phase end length

The presence of $C_\alpha(r)$ increases as r decreases. When $C_\alpha(r)$and are C_0 equal, v fall to zero, and GNPs stop growing. This r is called the critical radius . r_c According to Gibbs-Thomson formula:

$$\ln\frac{C_\alpha(r)}{C_\alpha}=\frac{2\gamma V_B}{RTr}=\frac{k}{r} \quad (6)$$

Where, γ is interface energy between α/β ; VB is the volume of the solute atom B.

The following formula can be obtained from (6)

$$C_\alpha(r)=C_\alpha\exp(\frac{k}{r})\ ;\quad C_0=C_\alpha(r_C)=C_\alpha\exp(\frac{k}{r_C})$$

As r and rC approach zero $\exp\left(\frac{k}{r}\right)=1+\frac{k}{r}$ $\exp\left(\frac{k}{r_C}\right)=1+\frac{k}{r_C}$;

So :

$$\frac{C_0 - C_\alpha(r)}{C_0 - C_\alpha} = \frac{C_\alpha \exp\left(\frac{k}{r_C}\right) - C_\alpha \exp\left(\frac{k}{r}\right)}{C_\alpha \exp\left(\frac{k}{r_C}\right) - C_\alpha} = \frac{\exp\left(\frac{k}{r_C}\right) - \exp\left(\frac{k}{r}\right)}{\exp\left(\frac{k}{r_C}\right) - 1}$$

$$== \frac{1 + \frac{k}{r_C} - 1 - \frac{k}{r}}{1 + \frac{k}{r_C} - 1} = 1 - \frac{r_C}{r} \quad (7)$$

It can be obtained from the above equation

$$C_0 - C_\alpha(r) = (C_0 - C_\alpha)\left(1 - \frac{r_C}{r}\right) \quad (8)$$

The formula (9) can be obtained by substituting (8) into (5).

$$v = \frac{D(C_0 - C_\alpha)}{Cr\left(C_\beta - C_\alpha\right)}\left(1 - \frac{r_C}{r}\right) \quad (9)$$

It can be seen from (9) that when the temperature is constant, the right side of the equation is a constant value, so the growth rate of the new phase of the flake has nothing to do with time.

In the actual transmission image of composite materials, both GNPs and TiC belong to the nanometer level. GNPs and TiC show a competitive growth trend during the whole cooling process. The former can be characterized by the diffusion coefficient of C atom in Ti melt, and the latter can be characterized by the volume fraction of TiC in Ti matrix. The diffusion reaction belongs to the multiphase diffusion reaction, that is, it goes along with the diffusion. Due to the composition change, reaction diffusion occurs simultaneously in the diffusion region [29]. It has the following characteristics:(1) the whole process is composed of two steps, diffusion and phase transformation, but diffusion is the controlling factor. Diffusion generally occurs in multiphase systems due to phase transition. (2) On the concentration-distance curve, the concentration distribution in the multiphase diffusion interval is discontinuous, and the concentration is abrupt at the phase boundary; (3) The formation of new phase in the multiphase system follows the phase law, that is, there is no mixed phase zone in the diffusion zone of binary alloy; (4) The formation of new phase corresponds to the phase diagram; (5) The dynamic law of new phase growth is that the broad band of phase region obeies parabola. In the actual cooling process, GNPs and TiC compete with each other and grow harmoniously. To convert carbon atoms into A,B, and G states. Because in the cooling process, a single layer of graphite will be the first out of segregation, and can be stable in a certain temperature range.

4.3. Enhancement mechanism

4.3.1. Interface structure

Figure 9 describes the interface structures of Ti, TiC and GNPs in the composite. The Ti-TiC-GNPS interface can be clearly seen. The two enhancers are distributed in a network, alternating between strong and weak. The average size of TiC is 20 nm, and the average size of GNPs is 10nm.One is the formation of titanium carbide between the substrate and GNPs (Figure 9). Another reason is that titanium carbide does not form between the matrix and GNPs. In the transition zone between GNPs and Titanium, the distance between TiC corresponding planes is 0.173 nm, corresponding to the (020) crystal plane of TiC. The grain plane Angle of Ti and TiC is 80.54°, which belongs to large Angle grain boundary. TEM diffraction specks in Figure 10 (a) show that there is no titanium carbide in the interface region, and the corresponding GNPs lamellar spacing is 0.35 nm, which belongs to three layers of graphene, which is consistent with the above Raman results. From the point of view of diffraction speckle, the diffraction speckle in the transition zone from titanium to GNPs has the characteristics of titanium and GNPs. The 0.254nm crystal plane spacing belongs to the (111) interface of titanium matrix and is parallel to the (001) crystal plane of graphene. The Angle between them is very small and belongs to the coherent relation. There are some amorphous structures in GNPs region. From the above analysis, it can be seen that the interface between Ti and GNPs is stable with obvious boundary. The interfacial structure keeps good plasticity while increasing strength.

View the image in Figure 10 (b) from the partition axis. Images clearly showing coherent twin boundaries and atomic arrangements confirm that they are indeed twins. Importantly, the two-atom steps on the coherent twin boundary are shown in Figure 10 (b). In addition, there are two monolayer steps on the coherent twin boundary. The most common twin system observed in HCP Ti is the deformation twin observed. This study is consistent with the twin pattern observed in the digital micrograph simulation.

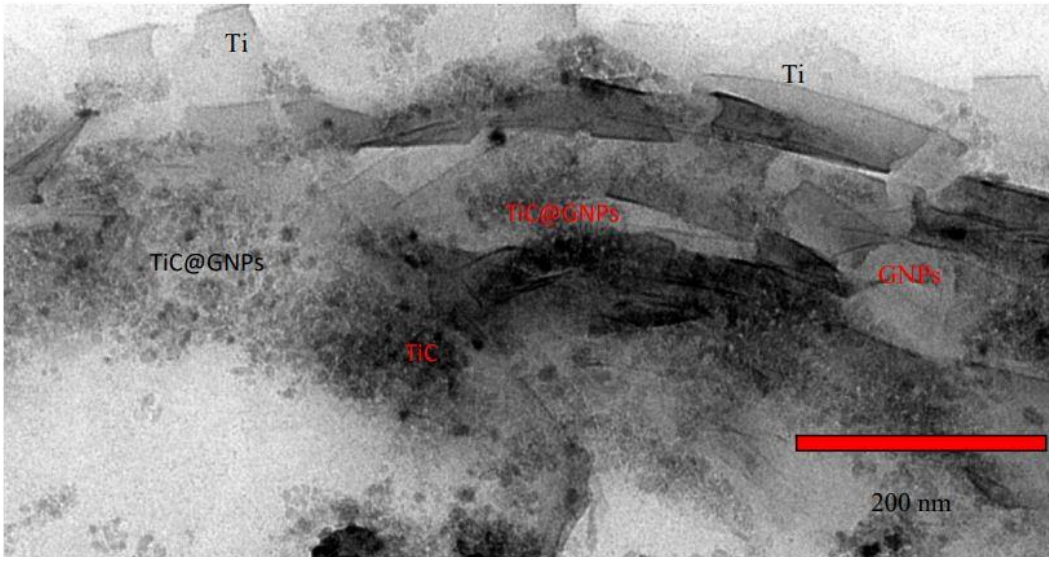

Figure 9: HRTEM micrograph of 0.25wt%TiC@GNPs/Ti composite under 1000°C HP process

Figure 9 TEM images of 0.25-1000-100-120 sample (where 0.25 is the mass content of the enhanced phase TiC@GNPs is 0.25% of the whole mass, 1000 is the sintering temperature of 1000°C, 100 heating rate of 100°C/min, and 120 holding time of 120 min.) It shows the reinforcement distribution inside the sample.

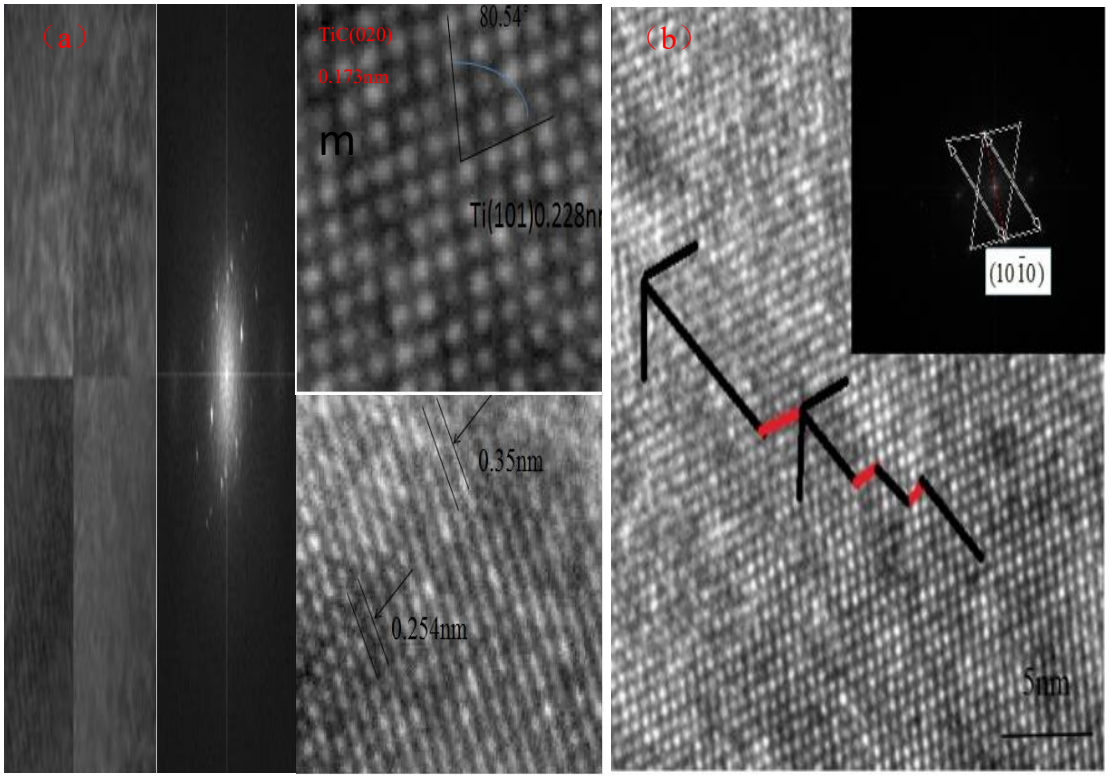

Figure 10 High resolution transmission electron microscope (HREM) images of TiC@GNPs area on the left in Figure 9 (a) HREM micrograph showing interface partitions of composite materials in (b) HREM micrograph showing a deformation twin in Fig.8(2), viewed along $(10\bar{1}0)$ zone axis. The twin system is . $\{10\bar{1}2\}\langle\bar{1}011\rangle$.

4.3.2. Enhancement mechanism

It is found that the superfine grain TiC@GNPs/Ti composite prepared by mechanical chemical ball milling and hot pressing sintering can not only significantly improve the strength of Ti matrix, but also increase the fracture strain by 3~5 times compared with the Ti alloy with similar superfine grain structure, indicating that the plasticity of the composite is greatly improved [29]. The introduction of in-situ reinforcing phase TiC@GNPs promotes the increase of Ti deformation. The structure of TiC@GNPs is a nano-layered structure formed by alternate arrangement of hard layer composed of TiC and soft layer composed of GNPs atoms, and the crack propagation is not easy to continue at TiC@GNPs/Ti, but tends to be in the interlayer. It can be analyzed that the plasticizing and toughening effects of TiC@GNPs are mainly as follows because of its own characteristics:

1. The low ductility of Ti at room temperature is related to its structural stability and its own slip system, while the in-situ generated TiC@GNPs has a good combination with the matrix Ti and significantly refined the grain. During compression deformation, TiC@GNPs can change the slip direction and reduce deformation resistance and stress concentration. The larger deformation can be obtained in the process of deformation [30].

2. TiC@GNPs is a "soft" reinforced phase, where dislocations TiC@GNPs cut through particles, and the fracture of the layered structure opens between layers, creating new surfaces that absorb large amounts of energy and improve the toughness of the material [31].

The semi-mechanical properties of this work were compared with those of titanium alloys with dual-scale structure reported in the literature. It can be seen that the comprehensive mechanical properties of the semi-solid sintered dual-scale titanium composite exceed the equilibrium trend reported in the current literature, and it has better yield strength and plastic strain. Therefore, the semi-solid sintering technology based on eutectic transition and the concept of microstructure and properties control proposed in this study provide a new way for the preparation of new dual-scale titanium alloys with high strength and toughness.

5. Conclusion

5.1. The semi-solid powder metallurgy technology of chemical mechanical ball milling + vacuum hot pressing sintering was used to successfully prepare TiC@GNPs reinforced pure titanium matrix composites. Compared with the existing research, the newly prepared titanium matrix composite has higher tensile strength and plasticity at room temperature, and good interface bonding, is potential in application. The uniform distribution of GNPs on the surface of large Ti powder was realized by using the 3d mechanical rotation mixing method.

5.2. With the increase of sintering temperature, the content of titanium carbide increases, and the yield strength and compressive strength of composites increase. The longer the heating time, the slower the heating rate and the lower the GNPs between titanium carbide ratio. High pressure and low temperature can reduce the reaction degree of GNPs, but a high proportion of GNPs residue does not bring significant improvement of mechanical properties. As the temperature increases, the heating rate decreases and TiC phase is more easily formed. With the change of heating rate and holding time, the microstructure does not change significantly. As the temperature increases, the holding time increases and the heating rate slows down, the reaction degree of GNPs with the matrix increases, but the compression performance increases with the reaction degree.

5.3.When the reaction degree of GNPs is very small, the interface strength cannot be guaranteed, while when the reaction degree is too high, the residual GNPs is very small, and TiC particles are coarsened, which limits the improvement of mechanical properties. There is an optimum proportion between GNPs and matrix. Among the samples explored in this experiment, for 0.25wt% TiC@GNPs, when the sintering temperature is 1 000℃, the heating rate is 100℃/min, and the temperature is 120 min, the reaction degree between GNPs and TiC reaches the best proportion, showing the best compression performance. The yield strength is 1086 MPa, the compressive strength is 1824 MPa, and the fracture strain is 41.3%. The three-dimensional network distribution of GNPs in titanium alloy matrix can regulate the contradiction between strength and plasticity of titanium matrix composites.

Authors' contributions

Zaiyu zhangand jianjun yang Complete the writing of the manuscript and the production of diagrams; yuan yang and liang cao Check the grammar of your manuscript; zaiqi zhang responsible for the article.

Acknowledgements

This research was supported by grains from the Hunan Provincial Key Laboratory Platform Construction Project of Dong Medicine Research (grant number 2017CT5025),the National Defense Science and Technology Key Laboratory Fund(6142005200305); Project (2022JJ50080) supported by the Natural Science Foundation of Hunan Province. We thank Jie Sun, Ming Yang and Sheng Yin for the technical assistance.

References

1. Tang, H., Huang, H., Liu, C., Liu, Z., & Yan, W. (2021). Multi-Scale modelling of structure-property relationship in additively manufactured metallic materials. International Journal of Mechanical Sciences, 194, 106185.
2. Kudryakov, O. V., Varavka, V. N., & Morozkin, I. S. (2020). Patterns of fracture initiation in metallic materials with a heterogeneous structure under dynamic cyclic loading. In Materials Science Forum (Vol. 989, pp. 127-132). Trans Tech Publications Ltd.
3. Schbel, M., Tolnai, D., Hofmann, M. (2021). Elasto-Plastic Deformation of Heterogeneous Metallic Materials: An Experimental Approach with AlMg4Si10[J].
4. Sun, Y., Li, P., Kauppinen, E. I., Sun, D. M., & Ohno, Y. (2022). Key factors for ultra-high on/off ratio thin-film transistors using as-grown carbon nanotube networks. RSC Advances, 12(25), 16291-16295.
5. Mathabathe, M. N., Govender, S., Bolokang, A. S., Mostert, R. J., & Siyasiya, C. W. (2018). Phase transformation and microstructural control of the α-solidifying γ-Ti-45Al-2Nb-0.7 Cr-0.3 Si intermetallic alloy. Journal of Alloys and Compounds, 757, 8-15.
6. Zhang, W., Zhou, S., Ren, W., Yang, Y., Shi, L., Zhou, Q., & Liu, M. (2021). Uniformly dispersing GNPs for fabricating graphene-reinforced pure Ti matrix composites with enhanced strength and ductility. Journal of Alloys and Compounds, 888, 161527.
7. Kang, L. M., Yang, C., Wang, F., Li, X. X., Zhu, D. Z., Zhang, W. W.... & Huan, Y. (2017). Designing ultrafine lamellar eutectic structure in bimodal titanium alloys by semi-solid sintering. Journal of Alloys and Compounds, 702, 51-59.
8. Sun, G., Chen, G., & Chen, G. (2007). Enhanced plasticity of Zr-based bulk metallic glass composite by in situ formed β-Zr dendritics. Frontiers of Materials Science in China, 1(1), 114-119.

9. Wei, D. X., Koizumi, Y., Nagasako, M., & Chiba, A. (2017). Refinement of lamellar structures in Ti-Al alloy. Acta Materialia, 125, 81-97.
10. Louzguine-Luzgin, D. V., Louzguina-Luzgina, L. V., Kato, H., & Inoue, A. (2005). Investigation of Ti–Fe–Co bulk alloys with high strength and enhanced ductility. Acta materialia, 53(7), 2009-2017.
11. Zhang, L. C., Das, J., Lu, H. B., Duhamel, C., Calin, M., & Eckert, J. (2007). High strength Ti–Fe–Sn ultrafine composites with large plasticity. Scripta materialia, 57(2), 101-104.
12. Wu X L, Yang M X, Yuan F P, et al. (2015). Heterogeneous lamella structure unites ultrafine- grain strength with coarse-grain ductility [J].Proc. Natl. Acad. Sci. USA, 112: 14501.
13. Yin, W. H., Xu, F., Ertorer, O., Pan, Z., Zhang, X. Y., Kecskes, L. J., ... & Wei, Q. (2013). Mechanical behavior of microstructure engineered multi-length-scale titanium over a wide range of strain rates. Acta materialia, 61(10), 3781-3798.
14. Long, Y., Guo, W. J., & Li, Y. (2016). Bimodal-grained Ti fabricated by high-energy ball milling and spark plasma sintering. Transactions of Nonferrous Metals Society of China, 26, 1170-1175.
15. Oketola, A., Jamiru, T., Adegbola, A. T., Ogunbiyi, O., Sadiku, R., & Salifu, S. (2022). Influence of sintering temperature on the microstructure, mechanical and tribological properties of ZrO2 reinforced spark plasma sintered Ni–Cr. International Journal of Lightweight Materials and Manufacture, 5(2), 188-196.
16. Huang, L., Geng, L., Li, A. B., Yang, F. Y., & Peng, H. X. (2009). In situ TiBw/Ti–6Al–4V composites with novel reinforcement architecture fabricated by reaction hot pressing. Scripta materialia, 60(11), 996-999.
17. Hashin, Z. S. H. T. R., & Shtrikman, S. (1962). A variational approach to the theory of the elastic behaviour of polycrystals. Journal of the Mechanics and Physics of Solids, 10(4), 343-352.
18. Song, Y., Chen, Y., Liu, W. W., Li, W. L., Wang, Y. G., Zhao, D., & Liu, X. B. (2016). Microscopic mechanical properties of titanium composites containing multi-layer graphene nanofillers. Materials & Design, 109, 256-263.
19. Tan, W., Jiang, X., Shao, Z., et al. (2022). Fabrication and mechanical properties of nanocarbon reinforced laminated Cu matrix composites [J]. Powder Technology, 395, 377-390.
20. Mu, X. N., Zhang, H. M., Cai, H. N., Fan, Q. B., Zhang, Z. H., Wu, Y., ... & Yu, D. H. (2017). Microstructure evolution and superior tensile properties of low content graphene nanoplatelets reinforced pure Ti matrix composites. Materials Science and Engineering: A, 687, 164-174.
21. Hu, Z., Chen, F., Xu, J., Ma, Z., Guo, H., Chen, C., ... & Zhang, M. (2018). Fabricating graphene-titanium composites by laser sintering PVA bonding graphene titanium coating: Microstructure and mechanical properties. Composites Part B: Engineering, 134, 133-140.
22. Mu, X. N., Cai, H. N., Zhang, H. M., Fan, Q. B., Wang, F. C., Zhang, Z. H., ... & Chang, S. (2018). Uniform dispersion and interface analysis of nickel coated graphene nanoflakes/pure titanium matrix composites. Carbon, 137, 146-155.
23. Sun, C., Zhang, X., Zhao, N. Q., et al. (2019). Influence of spark plasma sintering temperature on the microstructure and strengthening mechanisms of discontinuous three-dimensional graphene like network reinforced Cu matrix composites. Materials Science & Engineering A□756, 82-91.
24. Zhang, X., Shi, C., Liu, E., Zhao, N., & He, C. (2019). High-strength graphene network reinforced copper matrix composites achieved by architecture design and grain structure regulation. Materials Science and Engineering: A, 762, 138063.
25. Sun, S., & Lu, W. (2017). Effects of trace reinforcements on microstructure and tensile properties of in-situ synthesized TC18 Ti matrix composite. Journal of Composite Materials, 51(26), 3623-3629.
26. Cao, H. C., Liang, Y. L. (2020). The microstructures and mechanical properties of graphene-reinforced titanium matrix composites. Journal of Alloys and Compounds, 812, 152057.
27. Cao, Z., Wang, X., Li, J., Wu, Y., Zhang, H., Guo, J., & Wang, S. (2017). Reinforcement with graphene nanoflakes in titanium matrix composites. Journal of Alloys and Compounds, 696, 498-502.
28. Mu, X. N., Cai, H. N., Zhang, H. M., Fan, Q. B., Wang, F. C., Zhang, Z. H., ... & Wang, D. D. (2018). Uniform dispersion of multi-layer graphene reinforced pure titanium matrix composites via flake powder metallurgy. Materials Science and Engineering: A, 725, 541-548.
29. Fan, Y., Ye, L., Zhang, R., Guo, F., Tian, Q., Zhang, Y., & Li, X. (2021). Effects of 2D Ti3C2TX (Mxene) on mechanical properties of ZK61 alloy. Journal of Alloys and Compounds, 862, 158480.
30. Ge, Y. X., Zhang, H. M., Cheng, X. W., Fan, Q. B., Zhang, Z. H., Mu, X. N., ... & Wang, B. (2021). Interface evolution and mechanical properties of nickel coated graphene nanoflakes/pure titanium matrix composites. Journal of Alloys and Compounds, 853, 157157.
31. Guo, Y., Huang, J., Yu, K., Dai, G., Sun, Z., & Chang, H. (2022). Effect of the Ti-6Al-4V powder size on the microstructure and mechanical properties of composites with nickel-coated graphene nanoflakes. Materials Characterization, 184, 111627.
32. Das, G., Kestler, H., Clemens, H., & Bartolotta, P. A. (2004). Sheet gamma TiAl: status and opportunities. Jom, 56(11), 42-45.